Journal of Alloys and Compounds 509 (2011) 4505–4509

Contents lists available at ScienceDirect

Journal of Alloys and Compounds

journal homepage: www.elsevier.com/locate/jallcom

The effect of laser scanning path on microstructures and mechanical properties of laser solid formed nickel-base superalloy Inconel 718

Fencheng Liu, Xin Lin, Chunping Huang, Menghua Song, Gaolin Yang, Jing Chen, Weidong Huang*

State Key Laboratory of Solidification Processing, Northwestern Polytechnical University, Xi'an 710072, PR China

ARTICLE INFO

Article history:
Received 21 August 2010
Received in revised form
23 November 2010
Accepted 25 November 2010
Available online 3 December 2010

Keywords:
Laser solid form
Inconel 718
Scanning path pattern
Properties

ABSTRACT

Two kinds of laser scanning paths, i.e. single direction raster scanning (SDRS) and cross direction raster scanning (CDRS), were used to prepare Inconel 718 alloy parts by laser solid form (LSF) technology. The microstructures and mechanical properties of LSF Inconel 718 samples were investigated. It is shown that the as-deposited microstructure of SDRS sample is composed of columnar dendrites which grow epitaxially along the deposition direction; but in the CDRS sample, the continuous directional growth of columnar grains is inhibited and the orientation deviation of dendrites in two adjacent layers increases. The as-deposited grains of the CDRS sample are finer than those of the SDRS sample. After heat treatment, recrystallization occurs and grains of both samples are refined. However, the recrystallized grains in SDRS sample are not as uniform as that of the CDRS sample. Tensile testing at room temperature indicates that the ultimate tensile strength of these two samples is similar; however, the ductility of the CDRS sample is much better than that of the SDRS sample. Fracture surface examination presents a transgranular mode of crack propagation for the SDRS sample and a mixture of transgranular and intergranular modes of crack propagation for the CDRS sample. The inhomogeneity of grain size is considered to be the prime reason for the worse ductility of the SDRS sample.

1. Introduction

Laser solid form (LSF), which combines the laser cladding with rapid prototyping technique, is a novel technique developed to fabricate metal parts with full density, any geometries and high performance [1]. During LSF, a high power laser beam is focused onto the surface of the work piece to create a molten pool with high temperature which is above the melting point of its materials. Metal powders or wires are fed into the molten pool and melted rapidly when exposed to the high temperature liquid metal and the irradiation of high power laser beam. When the laser beam is moved away, the molten pool will re-solidify rapidly because the molten pool is very small compared with the work piece and heat can be dissipated away rapidly. By moving the laser beam following the pre-set path pattern, solid metal component can be formed point by point, line by line and layer by layer.

Many studies about the application of LSF in manufacturing of structures or components using different materials, such as stainless steels [1,2], titanium alloys [3,4], aluminum alloys [5] and nickel base superalloys [6–8], have been published. The mentioned studies have just concerned the investigations of the microstructures and mechanical properties of the metal work pieces or samples fabricated by LSF. However, the patterns of laser beam scanning path have scarcely been concerned in these studies, and especially rare data about the influence of laser beam scanning paths on microstructures and mechanical properties of LSF materials could be found in literatures till now. Laser beam scanning path pattern can influence the heat input and heat dissipation during LSF, and further influence the evolution of macrostructure and microstructure [9]. So in order to control its microstructures and properties, it is essential to study the differences in structures and properties of LSF structures or components deposited with different laser beam scanning paths.

In the present study, two kinds of laser scanning paths, i.e. single direction raster scanning (SDRS) and cross direction raster scanning (CDRS), were adopted to prepare Inconel 718 alloy parts by laser solid form (LSF) technology. The microstructures and mechanical properties of LSF Inconel 718 were investigated.

2. Experimental methods and materials

The LSF of Inconel 718 alloy samples was carried out on a LSF-I laser solid forming system consisted of a ROFIN-SINA 850 5 kW CO_2 laser, a controlled atmosphere chamber and a powder feeding system with a coaxial nozzle. Ar gas was used as shielding gas, which was also used to carry alloy powders into the molten pool and to protect the molten pool from oxidation. Inconel 718 alloy powders prepared by plasma rotation electrode process (PREP) method and with a size of about 150 μm and spherical shape were laser deposited on the low carbon steel sheet substrate. The

* Corresponding author. Tel.: +86 29 88494001; fax: +86 29 88494001.
E-mail address: huang@nwpu.edu.cn (W. Huang).

0925-8388/$ – see front matter © 2010 Elsevier B.V. All rights reserved.
doi:10.1016/j.jallcom.2010.11.176

Table 1
Processing parameters of LSF route.

Laser power (W)	Scanning velocity (mm/s)	Powder feeding rate (g/min)	Shielding gas flux (L/min)	Spot diameter (mm)	Overlap (%)	Increment of Z (mm)
2000–2200	6	5–8	4–8	3	40	0.3

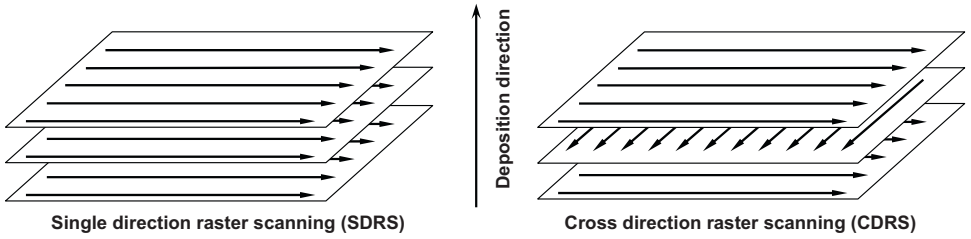

Fig. 1. Two kinds of laser scanning paths, i.e. single direction raster scanning (SDRS) and cross direction raster scanning (CDRS).

substrate surface was polished with sand paper and then was cleaned thoroughly with acetone before LSF. The LSF processing parameters are listed in Table 1. Two Inconel 718 alloy blocks were formed with two different laser beam scanning paths, i.e. single direction raster scanning (SDRS) and cross direction raster scanning (CDRS) respectively, but the same LSF processing parameters were used. Fig. 1 shows the schematic plans of SDRS and CDRS path patterns. The chemical composition of PREP powder and LSF material are listed in Table 2.

The LSF samples were cut and machined to small cubes or bars for microstructure observation, microhardness testing and tensile testing respectively. The heat treatment schedule is as follows: 1100 °C × 1.5 h/air cooling + 980 °C × 1 h/air cooling + 720 °C × 8 h and furnace cooling to 620 °C + 620 °C × 8 h/air cooling. For optical microscope (OM) microstructure observation, the specimens were prepared through the standard metallographic practice. Polished specimens were chemically etched with an etchant of a solution of 100 ml C_2H_5OH + 20 ml HCl + 5 g $FeCl_3$. Microhardness testing was conducted on an HX-1000TM Vickers microhardness tester with a load of 200 g and a dwell time of 20 s. Tensile testing of dumbbell-shaped standard tensile samples with a gauge length of 20 mm and a diameter of 3 mm was carried out at room temperature on an INSTRON11-3382 tensile testing machine. Fracture surface was characterized by a TESCAN VEGA II-LMH scanning electron microscope (SEM) to correlate the fracture characteristics with microstructures and mechanical properties.

3. Results and discussion

Fig. 2 shows the as-deposited microstructure in a cross section vertical to the laser beam scanning direction. The typical as-deposited microstructure of the LSF Inconel 718 alloy deposited using the SDRS path pattern presents the columnar dendrites growing epitaxially along the deposition direction, as shown in Fig. 2(a). Compared with Fig. 2(a), the microstructure of the as-deposited LSF Inconel 718 alloy deposited using the CDRS path pattern is obviously different, as shown in Fig. 2(b). The volume fraction of coarse columnar dendrites is reduced, and their growth directions are not as straight as that when SDRS path pattern was used. It is also found that the finer columnar grains and finer equiaxed grains are formed in most regions. Layer band structure like the arcs, which characterizes a single deposited track and layer, also can be seen in both Fig. 2(a) and (b).

Fig. 3 illustrates the heat dissipation and dendrite growth when SDRS and CDRS path patterns are used. During LSF, the heat is mainly dissipated through the pre-deposited layers, so that the heat flow direction during the solidification of molten pool is about perpendicular to the surface of pre-deposited layers, and in this direction the temperature gradient is the highest, which leads to the directional columnar dendrite solidification in the LSF specimen from the bottom up. It has been reported that directional solidification structure can be obtained by LSF method when the parameters are controlled accurately [10]. When a SDRS path pattern is used, the deposited path is same between the depositing layer and the previous deposited layer. The heat input and dissipation mode keep consistent when every path and every layer being deposited, which results in the good continuity for directional solidification characteristics. Meanwhile, due to the temperature gradient direction changing from the deposition direction at the bottom of molten pool to the scanning direction at the top of the molten pool, dendrites always grow preferably inclining towards the scanning direction resulting from the competitive growth of the dendrites, as shown in Fig. 3(a). Dendrite growth directions within two adjacent layers were the same and at last columnar grains are obtained which even pass several layers. When a CDRS path pattern is used, the laser beam scanning direction is normal to that of the previous deposited layer, so that the heat dissipation through the previous deposited part will change correspondingly, as well as the direction of the total temperature gradient. Thus, the dendrites, which grow preferably the previous deposited layer, will lose their growth superiority in the presented depositing layer, since their growth direction is largely deviated from the temperature gradient in the molten pool in the present depositing layer. The change of the preferred growth direction of the dendrites, even columnar to equiaxed transition (CET) [11,12], will occur in the present depositing layer, which depends on the deviation scale between the growth direction of the previous dendrites and the temperature gradient in the present depositing layer. The continuity of epitaxial growth of the dendrites is also broken as shown in Fig. 2.

Fig. 4 shows the microstructures of LSF Inconel 718 samples after heat treatment. Recrystallization occurs and equiaxed grains are formed in both samples deposited with SDRS and CDRS path patterns. It is shown that the average recrystallized grain sizes in these two samples are similar, but a greater difference between grain sizes exists in the SDRS sample than that in the CDRS sample. As shown in Fig. 4(a), the biggest grain size is larger than 500 μm and the smallest grain size is smaller than 50 μm in the recrystallized SDRS sample. However, the heat treated CDRS sample has a more uniform distribution of the grain size as shown in Fig. 4(b).

Table 2
Chemical compositions of LSF Inconel 718 superalloy (wt.%).

Elements	Cr	Fe	Ti	Al	Mo	Nb	C	Ni
LSF Inconel 718	19.3	18.4	0.9	0.3	3.7	5.8	0.031[a]	Balance
AMS:5663	17–21	16–20	0.65–1.15	0.2–0.8	2.8–3.3	4.75–5.5	0.08 max	Balance

[a] *Note:* The concentration of C element was analyzed by optical emission spectrometer, and others were obtained by energy dispersive X-ray spectrometer.

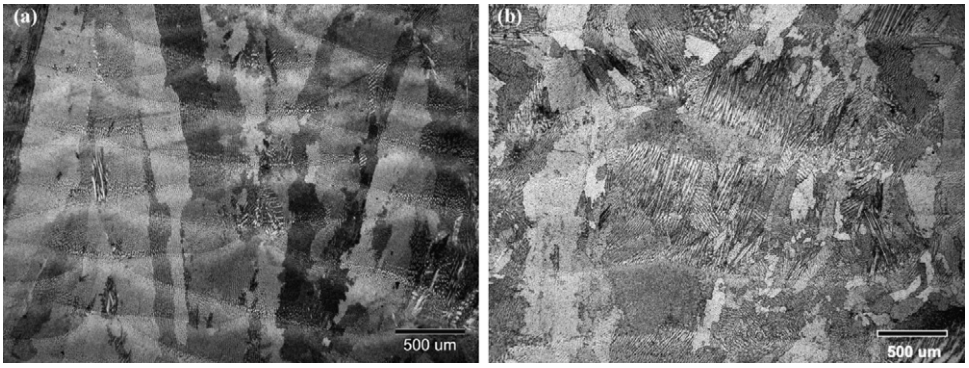

Fig. 2. Optic microscope graphs of as-deposited microstructures of LSF Inconel 718 alloy. (a) Deposited with single direction raster scanning (SDRS) and (b) deposited with cross direction raster scanning (CDRS).

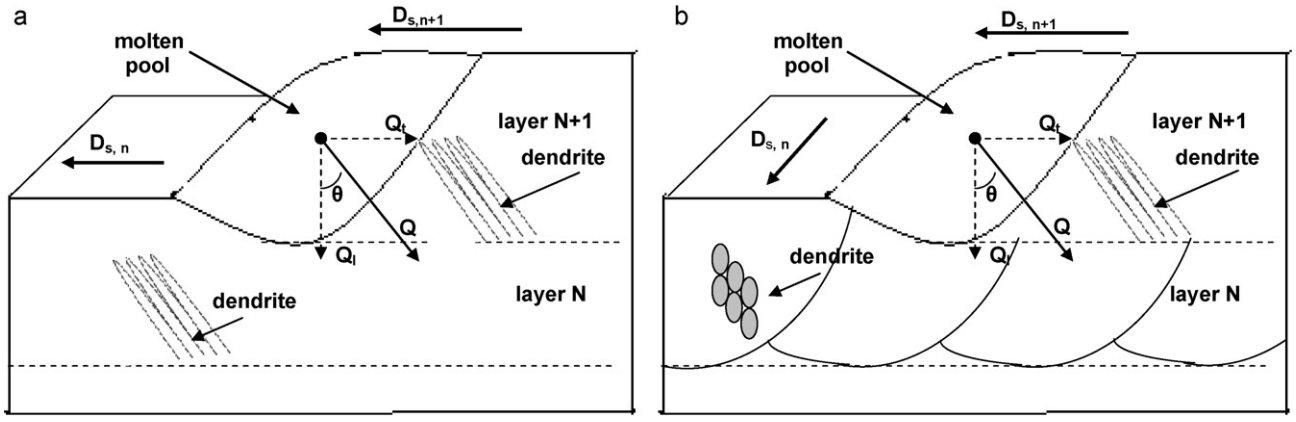

Fig. 3. Schematic plans of heat dissipation and dendrites growth when SDRS (a) and CDRS (b) path patterns were adopted. Q represents the heat dissipation direction, and Q_t, Q_l represent the transverse dissipation and longitudinal dissipation of heat respectively. $D_{s,n}$ represents the laser scanning direction in layer N, as well as the $D_{s,n+1}$.

The average grain size is about 100 μm, even if some large ones are larger than 200 μm. The grain size statistical results of recrystallized SDRS and CDRS samples are shown in Fig. 5. It is indicated that these two samples exhibit bi-modal size distributions, but the two distribution peaks of CDRS sample are all left to that of the SDRS sample, which means that the grain size of the former is smaller than the later.

The distribution of recrystallized grain sizes reflects the distribution of residual thermal stress. The previous study [13] has proved that the non-uniformly distributed recrystallized grain size is resulted from the uneven distributed residual thermal stress in micro-regions between the overlapping regions of two adjacent passes and the inner regions of single pass. So in the present study, the more uniform distributed grain size in the CDRS sample also indicates that its residual thermal stress distribution is more uniform than that of the SDRS sample.

Microhardness measurement also shows the differences in as-deposited samples deposited with two different path patterns. The series of points measured are in a straight line, which traverse two laser scanning paths within a single deposited layer, in a cross section perpendicular to the laser scanning direction, and with an interval of 100 μm between each other. For SDRS sample, only one line is measured, and for CDRS sample, two lines in two adjacent layers are measured. The statistical results are shown in Fig. 6. In general, the SDRS sample possesses higher microhardness than that of the CDRS sample. As shown in Fig. 6, almost 80% of the points measured have microhardness higher than 295HV in the SDRS sample, however, only less than 70% of the points measured, either in two adjacent layers, have a microhardness higher than 290HV in the CDRS sample. Same LSF process

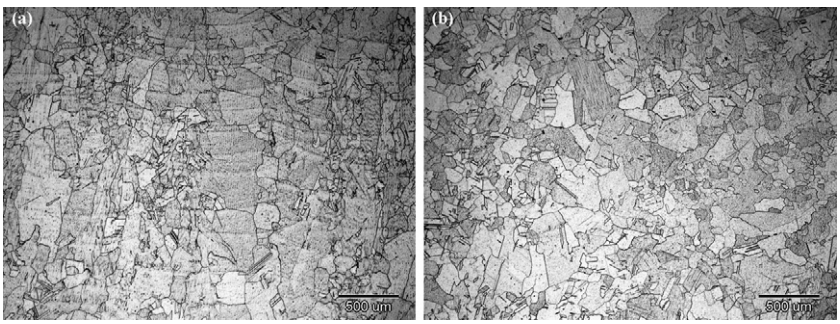

Fig. 4. Optic microscope graphs of recrystallized microstructures of LSF Inconel 718 alloy. (a) Deposited with single direction raster scanning (SDRS) and (b) deposited with cross direction raster scanning (CDRS).

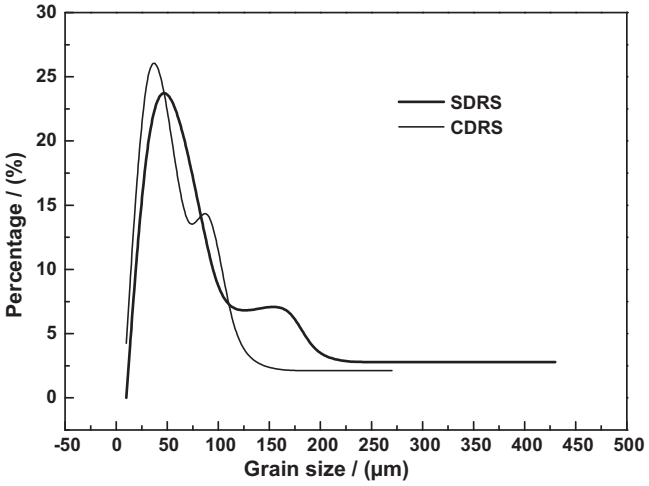

Fig. 5. Grain size statistical results of recrystallized SDRS and CDRS sample.

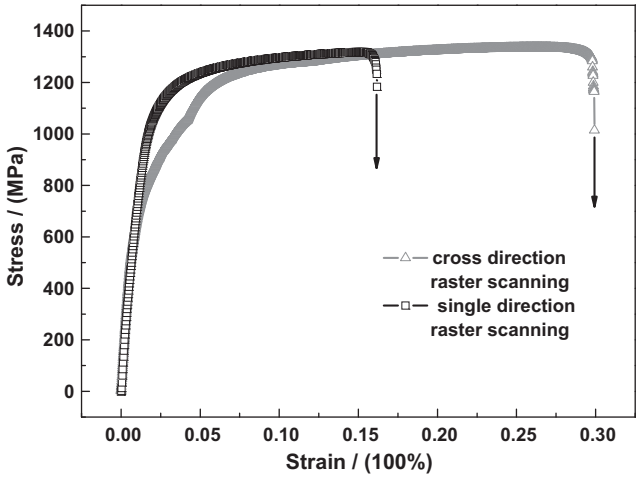

Fig. 7. Stress–strain curves of heat treated LSF Inconel 718 alloys tested at room temperature, showing the different tensile properties of samples deposited with different laser scanning path patterns.

parameters were used during LSF of these two samples as mentioned in Section 2. The heat input during the deposition of the upper layers has an annealing effect on the already deposited layers. It could be implied that, when CDRS path pattern is used, the areas undergo anneal covering the overlapping regions of two adjacent passes and the inner regions of single pass. However, when SDRS path pattern is used, only the inner regions of single pass, directly under the depositing pass, are annealed and the overlapping regions of two adjacent passes are not affected. Therefore, the statistical results show that the SDRS sample possesses a higher microhardness.

Fig. 7 shows the stress–strain curves of heat treated samples deposited with two different laser scanning path patterns in the tensile testing at room temperature. It is indicated that the yield stress of the SDRS sample is higher than that of the CDRS sample; meanwhile, their ultimate tensile stresses are similar. However, the ductility of the former is obviously lower than the later.

The major precipitates in Inconel 718 alloy are γ″ phase, γ′ phase and δ phase. γ″ phase and γ′ phase are the major strengthening phases which are coherent with the γ matrix. δ phase always precipitates at grain boundaries in the form of needle-like. δ phase is not coherent with the γ matrix and is reported having no strengthening effect to the γ matrix [14,15]. However, its appearance at grain boundaries can remove the notch sensitivity of the alloy. The different laser beam scanning path patterns used in the present study will also cause different residual stress in the as-deposited samples. Residual stress has been proved to have a certain influence on the precipitation of γ″ phase, γ′ phase and δ phase in Inconel 718 alloy [16,17]. However, the heat accumulation of every layer is similar for both samples; it is believable that the residual stress level is also similar for both the samples. Meanwhile, the identical heat treatment are used to these two samples, the precipitations of γ″ phase, γ′ phase and δ phase can also be reckoned to be in the same level, as well as their strengthening effects. So the difference in the stress–strain curves as shown in Fig. 7 is considered to be attributed to the difference in grain structure, in which the grain size difference of the SDRS sample is larger than that of the CDRS sample.

Fig. 8 illustrates the fractographs of the heat treated samples deposited with SDRS and CDRS path pattern. The crack initiation sites are all located near the surface areas as shown in Fig. 8(a) and (d), and high magnified images combined with EDS analysis show the presence of nonmetal inclusions in these areas. EDS analysis indicates that these nonmetal inclusions are mainly oxides inclusions which were formed during LSF. It also can be seen that the shear lip in SDRS sample is larger than that of CDRS sample, which indicates that the former represents the worse ductility than the later. Crack propagation occurred by a transgranular mode in SDRS sample and by a mixture of transgranular and intergranular modes in CDRS sample as shown in Fig. 8(b) and (e). In addition, both the fractographs of these two samples exhibit a considerable amount of dimples, which is the typical characteristic of ductile fracture as shown in Fig. 8(c) and (f).

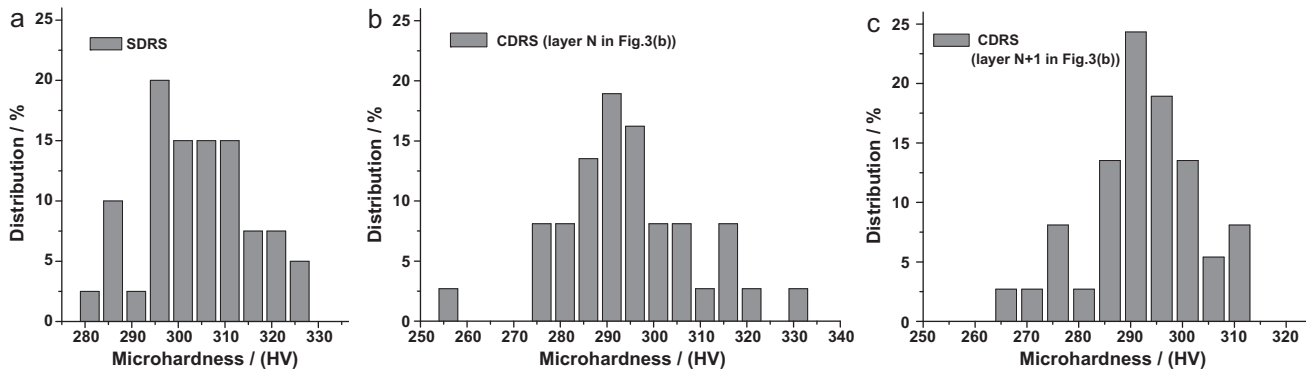

Fig. 6. Microhardness variations of as-deposited LSF Inconel 718 samples deposited with different laser scanning paths. (a) Deposited with single direction raster scanning (SDRS), (b) and (c) deposited with cross direction raster scanning (CDRS). (b) and (c) present the microhardness of two adjacent layers respectively.

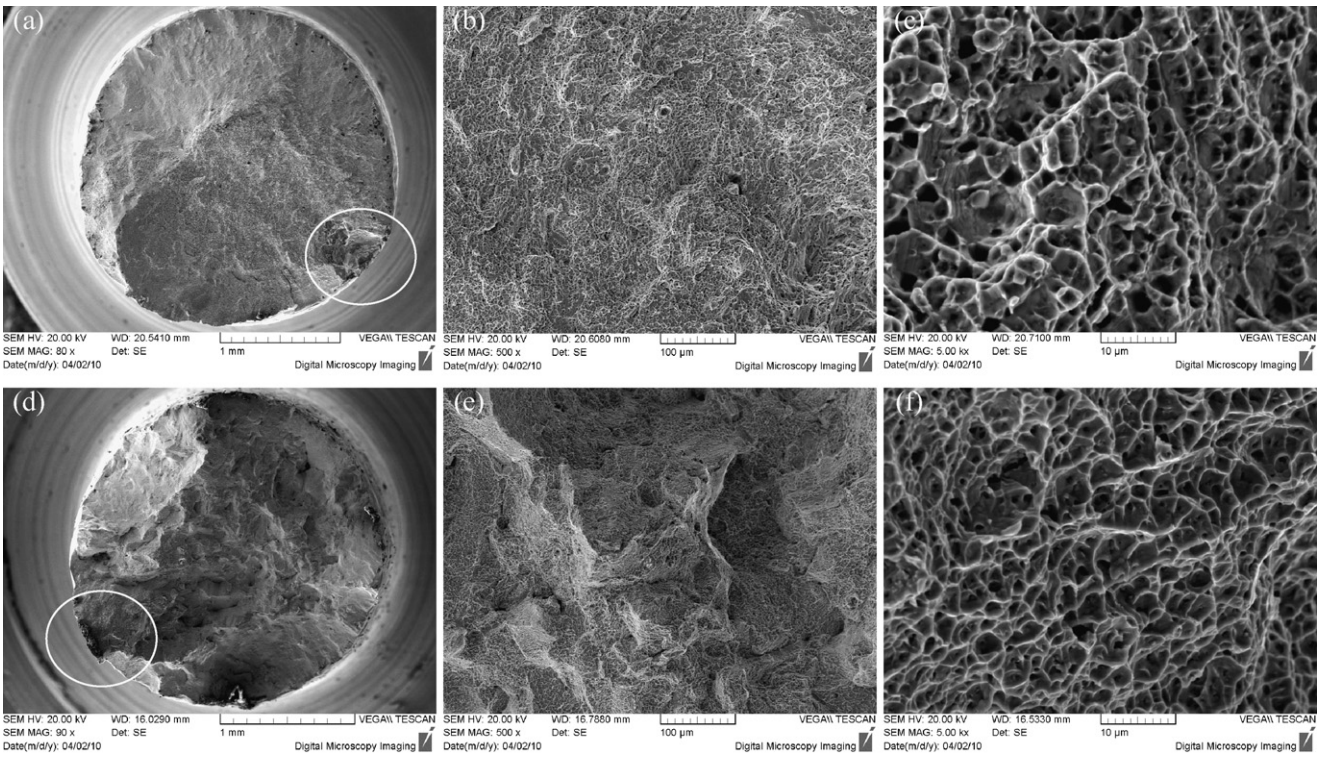

Fig. 8. Fracture surfaces of LSF Inconel 718 alloy. (a), (b) and (c) Fracture surface, crack propagation area and dimple pattern in crack propagation area of SRGS sample; (d), (e) and (f) fracture surface, crack propagation area and dimple pattern in crack propagation area of CRGS sample. Cycles show the initiation sites of each sample.

Ductility is affected by many aspects, such as precipitates, grain size and its orientation, grain boundary conditions, defects, etc. In this study, the precipitations of γ'' phase, γ' phase and δ phase are believed to be in the same level as mentioned above, as well as grain boundary condition. However, the grain size distributions are different between these two samples. Uneven deformation will occur in the non-isometric grains during plastic deformation, which leads to the different level of stress concentration and different dislocation densities in the adjacent grains with different size. And then different strain–hardening is induced for the different level of stress concentration. Larger grains are favorable cracks to propagate through owing to the weaker strain–hardening effect in these grains. The grain size of the SDRS sample is not as uniform as that of the CDRS sample after recrystallization. Thus, the ductility of SDRS sample is low and the crack propagation occurs by a transgranular mode.

4. Conclusions

(1) The as-deposited microstructure of SDRS sample is composed of columnar dendrites growing epitaxially along the deposition direction; but in respect of CDRS sample, the continuous directional growth of columnar grains was inhibited and an orientation deviation of dendrites in two adjacent layers increased.
(2) The grain size of the recrystallized SDRS sample is not as uniform as that of the recrystallized CDRS sample.
(3) The ultimate tensile strength of SDRS sample and CDRS sample was similar, and the ductility of the CDRS sample was better than the SDRS sample.
(4) The worse ductility of SDRS sample compared with the CDRS sample is considered to be resulted from the inhomogeneity of grain size.

Acknowledgements

This work was supported by the National Natural Science Foundation of China (NSFC) (Grant No. 50971102) and the National Basic Research Program of China (No. 2007CB613805), NPU Foundation for Fundamental Research (Grant No. NPU-FFR-JC200808), and the fund of the State Key Laboratory of Solidification Processing (NPU) (Nos. 16-TZ-2007 and 39-QZ-2009). The work is also supported by the Programme of Introducing Talents of Discipline to Universities (No. 08040).

References

[1] X. Lin, H.O. Yang, J. Chen, W.D. Huang, Acta Metall. Sin. 4 (2006) 361–368.
[2] J. Chen, X. Lin, T. Wang, H.O. Yang, W.D. Huang, Rare Metal Mater. Eng. 3 (2003) 183–186.
[3] S.Y. Zhang, X. Lin, J. Chen, W.D. Huang, Rare. Metal Mater. Eng. 5 (2009) 774–778.
[4] F.Y. Zhang, J. Chen, H. Tan, X. Lin, W.D. Huang, Chin. Opt. Lett. 3 (2009) 222–225.
[5] X.Y. Wang, J. Chen, X. Lin, F. Zhang, W.D. Huang, Chin. J. Lasers 6 (2009) 1585–1590.
[6] M. Anderson, R. Patwa, Y.C. Shin, Int. J. Mach. Tool. Manu. 46 (2006) 1879–1891.
[7] L. Sexton, S. Lavin, G. Byrne, A. Kennedy, J. Mater. Process. Technol. 122 (2002) 63–68.
[8] X.M. Zhao, X. Lin, J. Chen, L. Xue, W.D. Huang, Mater. Sci. Eng. A 504 (2009) 129–134.
[9] L. Ma, W.D. Huang, X.J. Xu, Rare Metal Mater. Eng. 10 (2009) 1731–1735.
[10] L.P. Feng, W.D. Huang, X. Lin, H.O. Yang, Chin. J. Nonferrous Metal 1 (2003) 181–187.
[11] W. Kurz, C. Bezencon, M. Gaumann, Sci. Technol. Adv. Mater. 2 (2001) 185–191.
[12] X. Lin, Y.M. Li, M. Wang, L.P. Feng, J. Chen, W.D. Huang, Sci. China Ser. E 5 (2003) 475–489.
[13] F.C. Liu, X. Lin, G.L. Yang, M.H. Song, J. Chen, W.D. Huang, Opt. Laser Technol. 43 (2011) 208–213.
[14] S. Azadian, L.Y. Wei, R. Warren, Mater. Charact. 53 (2004) 7–16.
[15] C. Slama, M. Abdellaoui, J. Alloys Compd. 306 (2000) 277–284.
[16] W.C. Liu, F.R. Xiao, M. Yao, Z.L. Chen, Z.Q. Jiang, S.G. Wang, Scripta Mater. 1 (1997) 52–57.
[17] Z.L. Chen, W.C. Liu, Strain-induced, Acta Metall. Sin. 2 (2000) 150–154.